ACS APPLIED MATERIALS & INTERFACES

Research Article

www.acsami.org

Ultrathin, Flexible Organic–Inorganic Hybrid Solar Cells Based on Silicon Nanowires and PEDOT:PSS

Manisha Sharma,[†] Pushpa Raj Pudasaini,[‡] Francisco Ruiz-Zepeda,[‡] David Elam,[‡] and Arturo A. Ayon*[,‡]

[†]Department of Chemistry and [‡]Department of Physics and Astronomy, University of Texas at San Antonio, One UTSA Circle, San Antonio, Texas 78249, United States

Supporting Information

ABSTRACT: Recently, free-standing, ultrathin, single-crystal silicon (c-Si) membranes have attracted considerable attention as a suitable material for low-cost, mechanically flexible electronics. In this paper, we report a promising ultrathin, flexible, hybrid solar cell based on silicon nanowire (SiNW) arrays and poly(3,4-ethylenedioxythiophene):poly(styrenesulfonate) (PEDOT:PSS). The free-standing, ultrathin c-Si membranes of different thicknesses were produced by KOH etching of double-side-polished silicon wafers for various etching times. The processed free-standing silicon membranes were observed to be mechanically flexible, and in spite of their relatively small thickness, the samples tolerated the different steps of solar cell fabrication, including surface nanotexturization, spin-casting, dielectric film deposition, and metallization. However, in terms of the optical performance, ultrathin c-Si membranes suffer from noticeable transmission losses, especially in the long-wavelength region. We describe the experimental performance of a promising light-trapping scheme in the aforementioned ultrathin c-Si membranes of thicknesses as small as 5.7 μm employing front-surface random SiNW texturization in combination with a back-surface distribution of silver (Ag) nanoparticles (NPs). We report the enhancement of both the short-circuit current density (J_{SC}) and the open-circuit voltage (V_{OC}) that has been achieved in the described devices. Such enhancement is attributable to the plasmonic backscattering effect of the back-surface Ag NPs, which led to an overall 10% increase in the power conversion efficiency (PCE) of the devices compared to similar structures without Ag NPs. A PCE in excess of 6.62% has been achieved in the described devices having a c-Si membrane of thickness 8.6 μm. The described device technology could prove crucial in achieving an efficient, low-cost, mechanically flexible photovoltaic device in the near future.

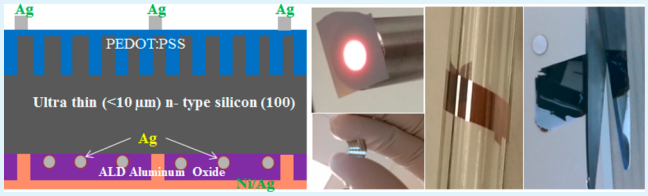

KEYWORDS: *solar cell, light trapping, flexible, ultrathin, plasmonics, conductive polymer, silicon nanowires*

1. INTRODUCTION

Photovoltaic (PV)—the conversion of sunlight into electricity—can potentially meet the rapidly growing demands for electric power with minimal deleterious environmental consequences. However, the real challenge can be ascribed to reducing the cost of solar cells while increasing their efficiencies. The high cost of single-crystal silicon (c-Si) structures originates on its poor IR absorption that arises from its indirect band gap, which has driven the geometry of currently marketed silicon-based solar cells to include a c-Si active layer of 180−300 μm thickness. This relatively thick layer is employed as the means to absorb light effectively and, hence, increase the device efficiency, but it also accounts for a significant portion of the total device cost. In order to address the challenge of bringing the cost down while attempting to achieve reasonable efficiencies, thin-membrane solar cells have been extensively characterized mostly because they are considered an alternative low-cost PV choice provided that the challenges of photon trapping and charge collection are judiciously addressed. Thus, free-standing c-Si thin membranes,[1−3] a suspended thin-film silicon-on insulator,[4−6] a thin c-Si film transfer layer,[7−9] silicon nanostructures including silicon nanowires (SiNWs),[10−16] silicon nanocones,[5,17−19] silicon nanoholes,[20−22] etc., have been considered as suitable alternatives for solar cell fabrication. However, light trapping in an ultrathin (<10 μm) c-Si membrane is one of the greatest challenges in solar cell technology because those membranes suffer significant reflection and transmission losses. Subwavelength nanoscale surface texturization is one of the approaches explored to enhance light absorption in such a thin c-Si membrane because of broad-band antireflection effects. Wang et al. have reported light-trapping effects by employing nanocone texturization of both surfaces in c-Si membranes with a thickness as small as 3 μm.[1] Similarly, other groups have reported light-trapping effects in thin c-Si membranes by utilization of nanometer-scale surface texturing both theoretically and experimentally.[10,19,21,23−28] Additionally, subwavelength metallic nanoparticles (NPs) have also attracted considerable attention for light-trapping purposes because they can induce localized surface plasmons (LSPs) that scatter incident light rather strongly into the thin active layer of a solar cell, thereby increasing the average path length inside the

Received: January 4, 2014
Accepted: February 25, 2014
Published: February 25, 2014

   dx.doi.org/10.1021/am500063w | ACS Appl. Mater. Interfaces 2014, 6, 4356−4363

device. LSPs are the collective oscillations of free electrons in the metallic NPs. In fact, metallic NPs interact strongly with visible and IR photons because of excitation of LSPs. The strongest optical interaction occurs at resonance, which is a function of the NP size, shape, and type of metal, as well as the local dielectric environment. Silver (Ag) NPs are commonly employed because of their relatively large scattering cross section and the potential for low photon absorption in the visible and near-IR (NIR) wavelengths. The plasmonic effect of metallic NPs on the PV performance has been reported elsewhere.[29−35] For example, Pillai et al. reported an overall photocurrent enhancement of 33% on a 1.25-μm-thick silicon-on-insulator wafer by depositing Ag NPs on the surface of the solar cells.[6] Ouyang et al. demonstrated a short-circuit current density (J_{SC}) enhancement of 27% on thin-membrane silicon solar cells employing self-assembled Ag NPs on the back surface of the devices.[31] Beck et al. reported a relative increase in the photocurrent of 10% for a 22-μm-thick silicon cell by incorporating self-assembled Ag NPs on the back surface of the device.[32] Tan et al. reported a net gain of 2 mA/cm^2 in the short-circuit current density without deterioration of the open-circuit voltage (V_{OC}) or the fill factor (FF) of the device by using Ag NPs as a plasmonic back reflector.[33]

In this paper, we describe a promising light-trapping scheme in a free-standing, ultrathin (<10 μm), mechanically flexible c-Si membrane by employing nanoscale front-surface texturing along with back-surface Ag NPs. The free-standing, ultrathin silicon membranes were produced by the aqueous potassium hydroxide (KOH) etching of double-side-polished silicon(100) wafers. The ultrathin membranes were observed to be mechanically flexible and sturdy enough to be handled with Teflon-coated tweezers. The front-surface nanoscale texturization exhibited noticeable broad-band antireflection effects, while the back-surface Ag NPs exhibited light-trapping effects in the long-wavelength regions. The described geometry is considered to be promising for the realization of efficient ultrathin devices, with a calculated enhancement of ∼140% in the short-circuit current density of a nanotexturized c-Si membrane of thickness 5.7 μm compared to a flat c-Si membrane with the same thickness. We fabricated the heterojunction hybrid solar cell on a sub-10-μm c-Si membrane by spin coating the organic polymer poly(3,4-ethylenedioxythiophene):poly(styrenesulfonate) (PEDOT:PSS). Organic−inorganic hybrid heterojunction solar cells are considered to be a viable alternative for low-cost PV devices because the Schottky junction between the inorganic and organic materials can be formed by employing relatively low temperature processing methods.[36−41] In conjunction with utilization of Al_2O_3, deposited by atomic layer deposition (ALD), as a back-surface passivation layer, we measured a power conversion efficiency (PCE) in excess of 6.62% for a device having a c-Si membrane thickness of 8.6 μm.

2. EXPERIMENTAL SECTION

2.1. SiNW Fabrication on Ultrathin Silicon Membranes. The vertically aligned SiNW arrays were fabricated on ultrathin silicon membranes, employing room-temperature, metal-assisted electroless chemical etching (MACE) methods. Originally, the n-type, double-side-polished, 4-in. silicon(100) wafers with a resistivity of 1−5 Ω·cm were cleaned in a piranha solution at 80 °C for 10 min. Subsequently, the substrates were rinsed with deionized (DI) water and dried with a nitrogen gun. Sub-10-μm free-standing silicon membranes of various thicknesses were obtained by immersing the wafers in a KOH solution with a concentration of 50 wt % at 90 °C for different amounts of time. Under these conditions, the observed silicon etching rate was ∼80 μm/h. The SiNW-array-textured surfaces were then produced by a modified two-step MACE method. Initially, Ag NPs were uniformly deposited on one side of the ultrathin silicon membranes while protecting the other side with Kapton tape and then immersing the samples in a solution comprising $AgNO_3$ (0.01 M) and HF (4.8 M) for 30 s. The SiNW arrays were then formed by immersing the samples coated with Ag NPs in an etching solution comprising H_2O_2, HF, and DI water in a volume ratio of 1:3:5. The mechanism of metal-assisted chemical etching of silicon can be found elsewhere.[42−45] The length of the SiNWs was controlled by the etching time. SiNWs of 2.10 μm length were obtained on the samples of different silicon membrane thicknesses by etching each sample for 90 s. The residual Ag NPs were then removed by immersing the samples in an aqueous HNO_3 solution for 10 min.

2.2. Synthesis of Spherical Ag NPs. Ag NPs of average size 90 nm were synthesized by a seed-mediated growth method as in ref [46]. To this end, 111 mg of poly(vinylpyrrolidone) (PVP) was added to 10 mL of diethylene glycol (DEG) while stirring at 80 °C. PVP acted as a capping agent. After the solution turned clear, 0.25 mL of a 0.5 M $AgNO_3$ aqueous solution was injected rapidly. The solution was maintained at 80 °C with continuous stirring until it turned yellow, and then the reaction solution was transferred to a 20 mL autoclave and heated at 230 °C for 24 h. Subsequently, the solution was allowed to cool to room temperature. Purification of the NPs was carried out by (i) filtration via a 200-nm-pore syringe filter followed by (ii) centrifugation at 2000 rpm for 15 min. Only the upper part of the solution was collected to obtain homogeneous Ag NPs of average size 90 nm. Finally, the recovered solution was washed several times with DI water to remove excess DEG.

2.3. ALD of Al_2O_3. ALD of Al_2O_3 was carried out with a Cambridge Nanotech Savanah 200 system. The substrate temperature was maintained at 120 °C during the deposition process. The precursors, trimethylaluminum and water, were kept at room temperature. Nitrogen (N_2) was used as a carrier and purge gas. ALD is a deposition process that employs cyclical self-limiting gas-surface reactions. This self-limiting reaction property is important for conformal deposition in high-aspect-ratio structures because of the time required for the reactant gases to fully diffuse into the narrow channels. The growth rate of this process over 100 cycles on a silicon(100) wafer with a native oxide, as measured by ellipsometry, was 0.9 Å/cycle. The index of refraction of the as-deposited AlO_x film was measured to be 1.71.

2.4. Solar Cell Fabrication. Prior to solar cell fabrication, the produced SiNW arrays on free-standing, ultrathin silicon samples went through a rigorous cleaning procedure. Initially, the samples were cleaned by immersing them in a piranha solution comprising H_2O_2 and H_2SO_4 in a volume ratio of 1:3 at 80 °C for 10 min. Subsequently, the samples were rinsed with DI water and dried with a N_2 gun. The samples were cleaned by immersing them in a solution consisting of H_2O_2 (30%), NH_4OH (37%), and DI water in a volume ratio of 1:1:5 at 80 °C for 30 min. The samples were then transferred to a DI water bath for 10 min. In the next step, the samples were immersed in a solution comprised of H_2O_2 (30%), HCl (37%), and DI water in a volume ratio of 1:1:5 at 80 °C for 30 min. Once more, the samples were then transferred to a DI water bath for 10 min. Finally, the samples were cleaned using a diluted HF (2%) solution for 60 s to remove native oxide. For back-side processing of the cell, the free-standing ultrathin c-Si membrane was taped on a dummy wafer using Kapton tape. Nickel (10 nm)/Ag (100 nm) finger electrodes connected to the bus line as a back contact were evaporated by utilizing a shadow mask. Then, a 10-nm-thick AlO_x film was deposited on the back side of the cells while protecting the bus line using Kapton tape. Ag NPs were self-assembled on the back surface of the c-Si thin-membrane sample by dispensing the previously prepared Ag NP aqueous solution. Afterward, another AlO_x film of 30 nm thickness was deposited on the back side to encapsulate the Ag NPs. Finally, a 300-nm-thick Ag film was evaporated on the back side of the cell to serve as the back-surface reflector. For front-side processing of the cell, the free-standing ultrathin silicon membrane was taped on a dummy wafer

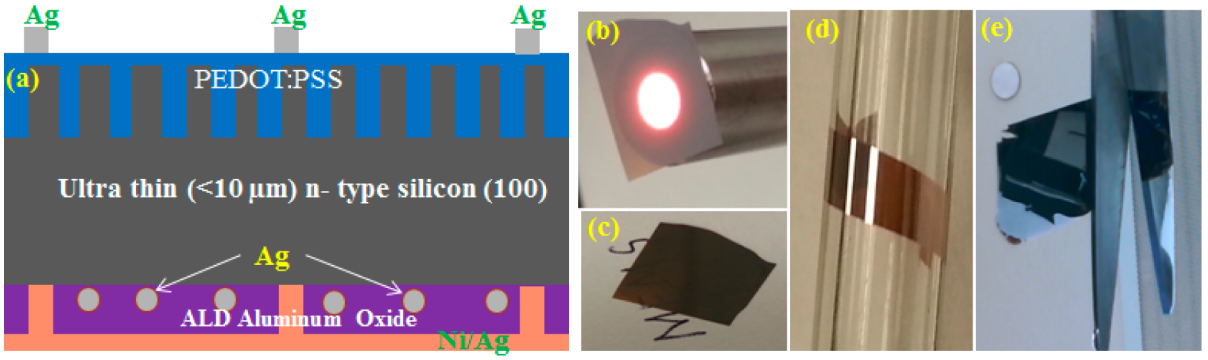

Figure 1. (a) Schematic illustration of the fabrication process of the described ultrathin, mechanically flexible silicon solar cells with a SiNW array on the front and plasmonic Ag NPs on the back. (b) Optical images of a free-standing, ultrathin silicon membrane, illuminated by white light from the back side. (c) Optical image of the produced ultrathin silicon membrane on top of white paper to verify the partial transparency of the membrane. (d) Ultrathin silicon membrane wrapped on a glass rod with a diameter of 5 mm. (e) Ultrathin silicon membrane being cut with scissors just like a piece of paper.

using Kapton tape. Then, highly conductive PEDOT:PSS (Sigma-Aldrich) mixed with a dimethyl sulfoxide and Triton X-100 solution (surfactant) was spin-cast at 300 rpm for 10 s and 2000 rpm for 60 s to form a core−shell radial heterojunction structure. The samples were then annealed on a hot plate at 140 °C for 30 min to remove the solvents. Finally, a 200-nm-thick Ag film was evaporated to form a finger grid connected to the bus bar as a front contact. Figure 1a depicts a schematic illustration of the fabrication of the described ultrathin, mechanically flexible silicon solar cells. We have fabricated three different devices having silicon membrane thicknesses of (a) 5.70, (b) 7.85, and (c) 8.6 μm as well as the corresponding planar reference solar cells for comparison purposes.

2.5. Characterization. The morphology of the samples was collected using high-resolution scanning electron microscopy (SEM; Hitachi S-5500) with a field-emission gun. Transmission electron microscopy (TEM) was used to obtain high-resolution images of the AlO_x film and the silicon interface in a JEOL 2010F TEM microscope operated at 200 kV. The cross-sectional TEM samples were prepared through a conventional mechanical polishing process including cutting, grinding, polishing, and a final ion-milling thinning step. The optical-reflectance spectral measurements were performed using a UV−vis−NIR (Varian cary-5000) spectrometer equipped with integrating spheres. The PV measurements were performed using a solar simulator (Newport Sol2A) under AM 1.5G illumination (1000 W/m^2) at standard testing conditions. Prior to real sample measurement, the simulator intensity was calibrated with a reference cell from Newport (Irvine, CA) to ensure that the irradiation variation was within 3%.

3. RESULTS AND DISCUSSION

3.1. Device Characterization. Figure 1b is an optical image of the free-standing c-Si membrane of thickness 5.7 μm with underneath light illumination. In Figure 1c, because of insufficient light absorption, a fraction of the scattered light is transmitted through a membrane lying on a piece of paper. The wavelength of light corresponding to the absorption depth of 5.7 μm is around 710 nm for 1 skin depth; therefore, light with a wavelength greater than 710 nm was insufficiently absorbed. Figure 1d shows a c-Si thin membrane of thickness 5.7 μm wrapped around a glass tube of 5 mm diameter because the sub-10-μm free-standing membrane is mechanically flexible and sturdy enough to tolerate handling with Teflon-coated tweezers and the rigors of clean-room processing including texturization, spin-casting, dielectric film deposition, and metallization. It can also be cut with scissors (see Figure 1e and Supporting Information videos S1 and S2).

Parts a−c of Figure 2 are cross-sectional SEM micrographs of the vertically aligned SiNW arrays on samples with different

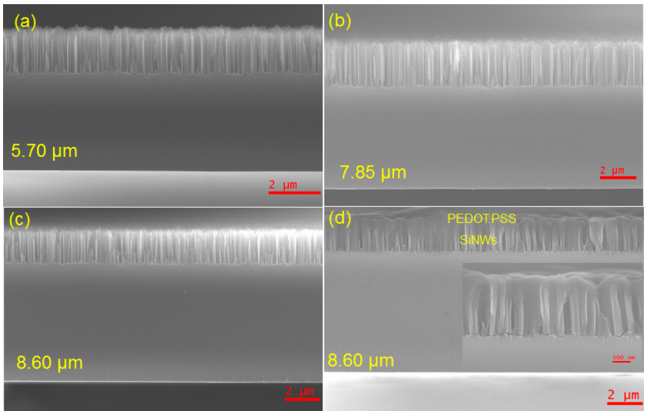

Figure 2. Cross-sectional SEM micrographs of SiNW arrays on an ultrathin c-Si membrane with different membrane thicknesses of (a) 5.70, (b) 7.85, and (c) 8.6 μm produced by KOH etching of silicon wafers. The vertically aligned SiNW arrays were produced by Ag-NP-assisted chemical etching of silicon. (d) Cross-sectional SEM image of the PEDOT:PSS-coated SiNW-array-textured sample. The image in the inset is a higher magnification image of the same sample with a scale bar of 500 nm.

thicknesses, namely, (a) 5.70, (b) 7.85, and (c) 8.6 μm. SiNWs of 2.11 μm length were obtained for a texturization time of 90 s using Ag-catalyzed electroless chemical etching methods. Figure 2d is the cross-sectional SEM image of the PEDOT:PSS-coated SiNW array on an ultrathin c-Si membrane, forming a radial p−n junction. The image in the inset of Figure 2d is a higher magnification image of the same sample showing infiltration of PEDOT:PSS on the SiNW-array-textured surface. Figure 3a is a SEM micrograph of the spherical Ag NPs of the average size of 90 nm synthesized by a seed-mediated growth method. The particle size distribution is shown in Figure 3b. Figure 4a is the cross-sectional SEM micrograph of a fabricated device. Figure 4b shows the rear surface of the same device with Ag NPs embedded on an AlO_x passivation layer. The inset in the lower left corner of Figure 3b shows the embedded Ag NPs in 30 nm ALD-deposited AlO_x, while the inset in the upper right corner of the same figure is a high-resolution TEM micrograph of the Si/AlO_x interface.

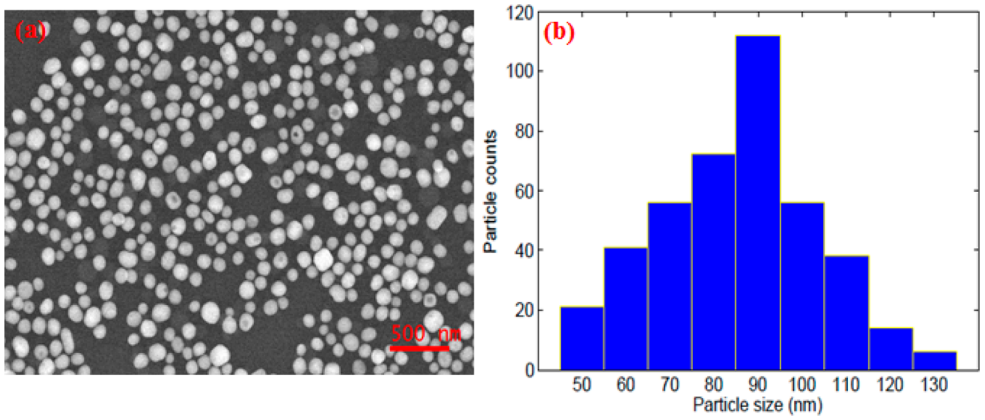

Figure 3. (a) SEM micrograph of the synthesized spherical Ag NPs. (b) Particle size distributions of Ag NPs.

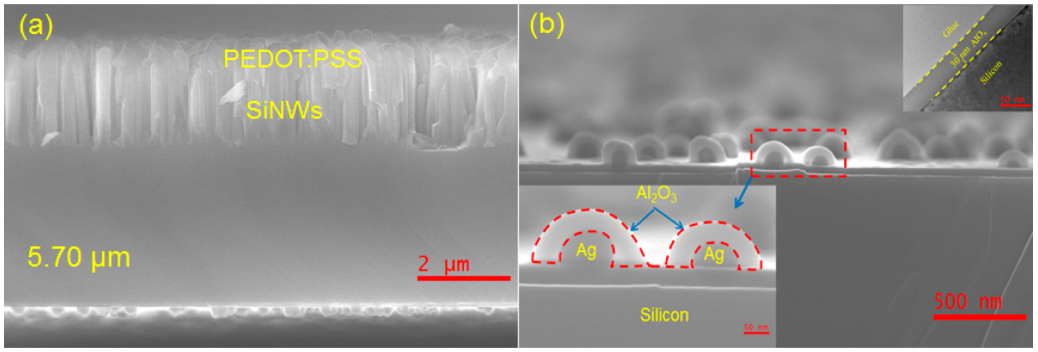

Figure 4. (a) Cross-sectional SEM micrograph of the described device with the PEDOT:PSS-coated SiNW-textured surface on the front and an array of Ag NPs embedded in an AlO_x dielectric layer on the back side of the device. (b) Higher-magnification cross-sectional SEM micrographs of the back side of the same device showing the Ag NPs coated with ALD-deposited AlO_x. The inset in the upper right corner is the TEM image of the silicon AlO_x interface.

3.2. Light-Trapping Performance of the Device. Light trapping in an ultrathin (<10 μm) c-Si membrane is one of the greatest challenge for the realization of an efficient solar cell. The ultrathin c-Si membrane suffers from significant reflection and transmission losses. Subwavelength nanoscale surface texturing is one of the promising approaches to enhance light absorption because of broad-band antireflection effects. Moreover, plasmonic metal NPs have the potential to further enhance optical absorption due to LSP resonances. We experimentally measured the light-trapping performance of the described device having front-surface SiNW array texturing and back-surface Ag NPs. The absorption spectra was calculated from the measured reflection and transmission spectra employing the relation $A = 100 - (R + T)$.

Parts a–c of Figure 5 show the absorption spectra of (i) a plane silicon membrane without texturization (in red), (ii) front-surface SiNW array texturing only (in blue), and (iii.) front-surface SiNW array texturing in combination with back-surface Ag NPs (in green) for three different membrane thicknesses, namely, 5.70 μm in Figure 5a, 7.85 μm in Figure 5b, and 8.6 μm in Figure 5c, respectively. The observations indicate that the front-surface SiNW array texturization (in blue) has a noticeable absorption enhancement over the entire wavelength range compared to the samples without texturization (in red). The addition of the back-surface Ag NPs further improves the absorption performance for all devices particularly in the long-wavelength region because of plasmonic back-scattering of light by Ag NPs (green curves in Figure 5a–c). To further quantify the absorption performance of the different geometries of the described devices, we calculated the short-circuit current density from the measured absorption spectra assuming a 100% internal quantum efficiency for each device by using the equation

$$J_{SC} = \int_0^{\lambda_g} I(\lambda)\, A(\lambda)\, \frac{e\lambda}{hc}\, d\lambda \qquad (1)$$

where $A(\lambda)$ is the measured absorption spectra of the ultrathin sample, $I(\lambda)$ is the air mass 1.5G solar spectrum,[47] and λ is the wavelength of the incident light. The front-surface SiNW array texturization has a beneficial effect on the photocurrent generation for all membrane thicknesses. Specifically, because of utilization of front-surface SiNW array texturization, J_{SC} increases from 14.64 to 35.08 mA/cm^2 in the c-Si thin membrane of a thickness of 5.7 μm and from 19.94 to 36.10 mA/cm^2 in the c-Si membrane with a thickness of 8.60 μm. Utilization of back-surface Ag NPs further improves the photocurrent when employed in conjunction with the front-surface SiNW texturization; specifically, for the c-Si membrane of a thickness of 5.7 μm, J_{SC} increases from 35.08 to 36.14 mA/cm^2, while for the relatively thicker 8.6 μm membrane, the value of J_{SC} increases to 36.51 mA/cm^2 from 36.10 mA/cm^2. Therefore, the described light-trapping scheme comprising SiNW and Ag NPs is considered promising in view of the increase in the short-circuit current density. For instance, in the case of a 5.7-μm-thick c-Si sample, J_{SC} was observed to increase from 14.64 mA/cm^2 for a flat sample to the noticeably higher 36.51 mA/cm^2 for a sample with the aforementioned light-trapping scheme.

dx.doi.org/10.1021/am500063w | ACS Appl. Mater. Interfaces 2014, 6, 4356–4363

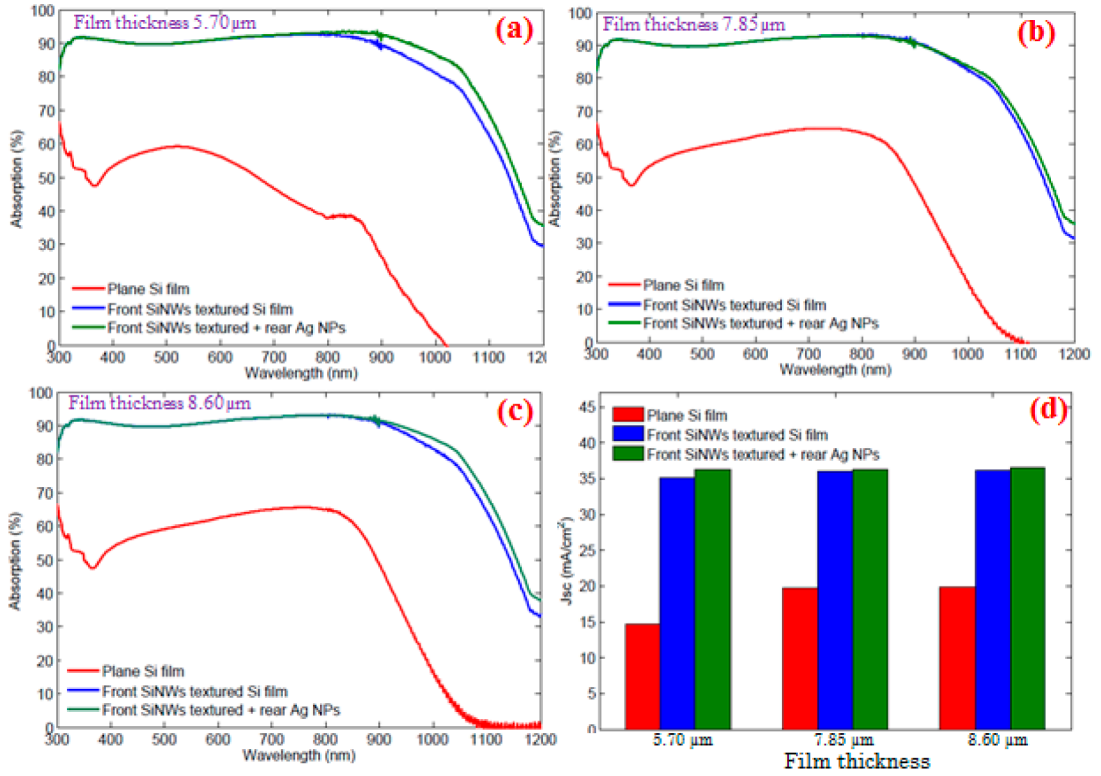

Figure 5. Absorption spectra of ultrathin silicon membranes with a plane surface (no texturing), front-side SiNWs textured, and front SiNWs textured with back-surface Ag NPs, for different membrane thicknesses of (a) 5.70, (b) 7.85, and (c) 8.6 μm. (d) Short-circuit current density enhancement calculated from the measured absorption spectra assuming a 100% internal quantum efficiency for three different membrane thicknesses (i.e., 5.70, 7.85, and 8.60 μm). The red, blue, and green bars in the bar diagram correspond to the plane (no texturing), front-surface SiNWs textured, and front-surface SiNWs textured with back-surface plasmonic Ag NPs, respectively.

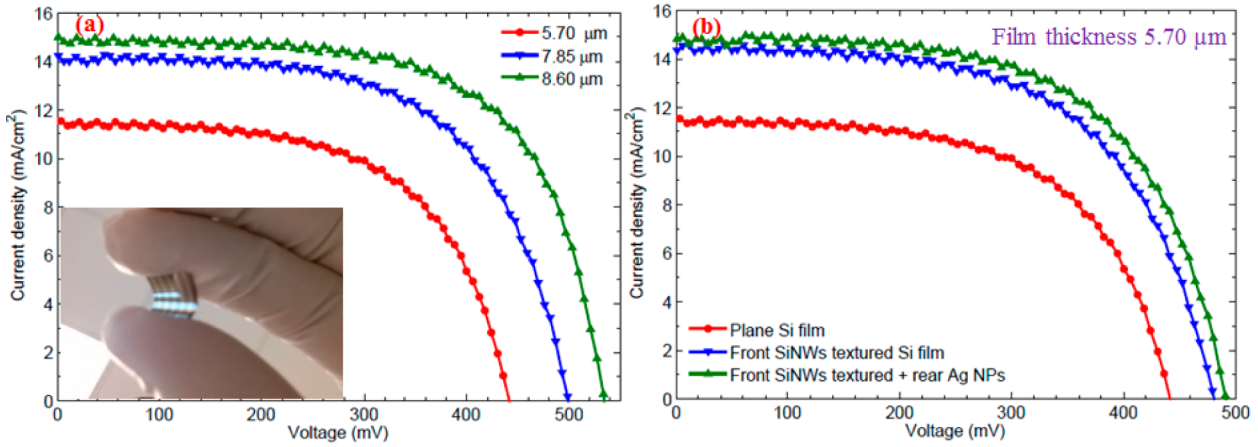

Figure 6. (a) Current density versus voltage curves for three different planar silicon hybrid solar cells with membrane thicknesses of 5.70, 7.85, and 8.60 μm. The inset in the lower left corner is an optical image of a test sample with dimensions of 1.2 cm × 1.2 cm. (b) Comparison of the $J-V$ curves for ultrathin samples of 5.70 μm thickness having (i) no texturization (in red), (ii) front-surface SiNW texturization (in blue), and (iii) front-surface SiNW texturization with back-surface Ag NPs (in green). Both J_{SC} and V_{OC} increase noticeably with front-surface SiNW array texturization, and they are further improved with the addition of rear back-surface plasmonic Ag NPs.

3.3. PV Performance of the Device. Inorganic semiconductors and organic-conjugated polymers can be advantageously combined to demonstrate a possible alternative route to enable low-cost, hybrid PV devices. We fabricated the heterojunction hybrid solar cells on an ultrathin silicon membrane by spin-casting the conductive organic polymer PEDOT:PSS on the previously prepared ultrathin samples. Solar cells with three different geometries were fabricated, namely, (a) a flat surface (no texturing), (b) a front SiNW-array-textured surface and (c) front SiNW array texturization with back-surface Ag NPs, in three different membrane thicknesses (i.e., 5.70, 7.85, and 8.60 μm, respectively).

Figure 6a shows the current density versus voltage ($J-V$) curves of the flat, ultrathin, hybrid solar cells having different membrane thicknesses under AM 1.5G illumination. The inset in the lower left corner depicts the optical image of the test sample with dimensions of 1.2 cm × 1.2 cm. The values of both J_{SC} and V_{OC} were observed to increase as the membrane

dx.doi.org/10.1021/am500063w | ACS Appl. Mater. Interfaces 2014, 6, 4356−4363

thickness increased. Thus, J_{SC} and V_{OC} values of 534 mV and 15.05 mA/cm^2, respectively, were collected, leading to a calculated PCE of 5.20% for the 8.60-μm-thick c-Si membrane, while the corresponding values of J_{SC} and V_{OC} of 446 mV and 11.47 mA/cm^2, respectively, were obtained for the relatively thinner cell of 5.70 μm thickness, producing a PCE of 3.41%. The 5.70-μm-thick cell suffers from a relatively higher transmission loss as well as a higher surface recombination, which are responsible for an inferior PV performance compared to the thicker cell. Similar results have been reported by Wang et al.[1]

Figure 6b shows the $J-V$ curves for the devices having a c-Si membrane thickness of 5.70 μm but with different solar cell geometries, namely, a flat surface (in red), a front SiNW-array-textured surface (in blue), and front SiNW arrays textured with back-surface Ag NPs (in green). The PV performance parameters of all fabricated devices including J_{SC}, V_{OC}, FF, and PCE are summarized in Table 1.

Table 1. Average PV Property of the Ultrathin, Heterojunction, Hybrid Solar Cells with Different Cell Geometries

thickness (μm)	cell type	V_{OC} (mV)	J_{SC} (mA/cm^2)	FF (%)	PCE (%)
5.70	planar	446	11.47	67.16	3.41
	front SiNP textured	480	14.71	62.05	4.16
	front SiNP textured with back Ag NPs	492	14.97	62.23	4.58
7.85	planar	499	14.30	68.08	4.85
	front SiNP textured	524	17.38	63.27	5.72
	front SiNP textured with back Ag NPs	529	17.40	65.6	6.02
8.60	planar	534	15.06	64.93	5.20
	front SiNP textured	542	18.30	63.8	6.33
	front SiNP textured with back Ag NPs	545	18.50	65.5	6.62

The values of both J_{SC} and V_{OC} improved with utilization of front-surface SiNW array texturization irrespective of the membrane thickness. The broad-band antireflection effects of the SiNW arrays were directly observed on the measured values of J_{SC} of the devices. Case in point, J_{SC} increased to 14.97 mA/cm^2 from 11.47 mA/cm^2 on the silicon membrane sample of 5.7 μm thickness. Similarly, the values of J_{SC} and V_{OC} of 18.30 mA/cm^2 and 542 mV were obtained on the silicon thin-membrane sample of thickness 8.60 μm having a front-surface SiNW array texturization, leading to a PCE value of 6.33%, which compares favorably to the PCE value of 5.20% for a flat device with the same thickness. Utilization of back-surface Ag NPs further improves the electrical performance of the described devices. For instance, the values of J_{SC} and V_{OC} of 480 mV and 14.70 mA/cm^2, respectively, were obtained for the device with a membrane thickness of 5.70 μm with front-surface SiNW texturization only, and these values were observed to increase to 492 mV and 14.97 mA/cm^2, respectively, leading to a ~10% overall increase in PCE of the device. Similarly, for the 8.6-μm-thick sample, PCE of the device increased from 6.33% to 6.62% because of utilization of the Ag NPs on the back surface. This can be attributed to plasmonic back-scattering of photons by Ag NPs.

Prior to Ag NP dispersion, the back surfaces of all thin-membrane silicon samples were passivated with a 10-nm-thick Al_2O_3 film; this is relevant because surface recombination is high for such a thin sample. Furthermore, the FF of the SiNW-texturized devices improves with the presence of Ag NPs embedded in the dielectric passivation layer (see Table 1) because of the relatively low value of the measured series resistance compared to those devices without the NPs. The performance of the described devices can be further improved by optimization of (a) the SiNW array morphology, (b) the interfacial passivation between the SiNW-textured surface and the PEDOT:PSS layer, (c) the thickness of the dielectric spacer layer between Ag NPs and the silicon surface, (d) the size and density of Ag NPs, and (e) front and rear contact electrodes, among others.

4. CONCLUSIONS

PCE in excess of 6.62% has been observed in a c-Si heterojunction hybrid solar cell of 8.6 μm thickness with a topography that included a SiNW array used in conjunction with the organic semiconductor PEDOT:PSS. Additional samples of thicknesses of 5.7 and 7.85 μm have also been fabricated and characterized. The experimental observations support the promising light-trapping effects in an ultrathin c-Si membrane when employing front-surface random SiNW texturization in combination with back-surface Ag NPs. The enhancement in both the short-circuit current density and the open-circuit voltage measured in the described devices is due to the plasmonic back-scattering effects of Ag NPs on the back surface, leading to an overall 10% increase in PCE compared to similar devices with SiNW texturization but without Ag NPs. The described device technology could prove to be crucial to achieve a low-cost, mechanically flexible, PV device in the near future.

■ ASSOCIATED CONTENT

Supporting Information

Videos S1 and S2 showing the processing approach of the fabricated ultrathin c-Si membrane. This material is available free of charge via the Internet at http://pubs.acs.org.

■ AUTHOR INFORMATION

Corresponding Author

*E-mail: aayon@utsa.edu. Phone: 210-458-7245.

Notes

The authors declare no competing financial interest.

■ ACKNOWLEDGMENTS

We thank the U.S. Army Research Office for financial support provided for this project under Grant W911NF-13-1-0110.

■ REFERENCES

(1) Wang, S.; Weil, B. D.; Li, Y.; Wang, K. X.; Garnett, E.; Fan, S.; Cui, Y. Large-area free-standing ultrathin single-crystal silicon as processable materials. *Nano Lett.* **2013**, *13*, 4393−4398.

(2) Yoon, J.; Baca, A. J.; Park, S. I.; Elvikis, P.; Geddes, J. B., 3rd; Li, L.; Kim, R. H.; Xiao, J.; Wang, S.; Kim, T. H.; Motala, M. J.; Ahn, B. Y.; Duoss, E. B.; Lewis, J. A.; Nuzzo, R. G.; Ferreira, P. M.; Huang, Y.; Rockett, A.; Rogers, J. A. Ultrathin silicon solar microcells for semitransparent, mechanically flexible and microconcentrator module designs. *Nat. Mater.* **2008**, *7*, 907−915.

(3) Wang, K. X.; Yu, Z.; Liu, V.; Cui, Y.; Fan, S. Absorption enhancement in ultrathin crystalline silicon solar cells with antireflection and light-trapping nanocone gratings. *Nano Lett.* **2012**, *12*, 1616−1619.

(4) Mavrokefalos, A.; Han, S. E.; Yerci, S.; Branham, M. S.; Chen, G. Efficient light trapping in inverted nanopyramid thin crystalline silicon membranes for solar cell applications. *Nano Lett.* **2012**, *12*, 2792−2796.
(5) Lu, Y.; Lal, A. High-efficiency ordered silicon nano-conical-frustum array solar cells by self-powered parallel electron lithography. *Nano Lett.* **2010**, *10*, 4651−4656.
(6) Pillai, S.; Catchpole, K. R.; Trupke, T.; Green, M. A. Surface plasmon enhanced silicon solar cells. *J. Appl. Phys.* **2007**, *101*, 093105(1)−093105(8).
(7) Cruz-Campa, J. L.; Okandan, M.; Resnick, P. J.; Clews, P.; Pluym, T.; Grubbs, R. K.; Gupta, V. P.; Zubia, D.; Nielson, G. N. Microsystems enabled photovoltaics: 14.9% efficient 14μm thick crystalline silicon solar cell. *Sol. Energy Mater. Sol. Cells* **2011**, *95*, 551−558.
(8) Saha, S.; Hilali, M. M.; Onyegam, E. U.; Sarkar, D.; Jawarani, D.; Rao, R. A.; Mathew, L.; Smith, R. S.; Xu, D.; Das, U. K.; Sopori, B.; Banerjee, S. K. Single heterojunction solar cells on exfoliated flexible ∼25 μm thick mono-crystalline silicon substrates. *Appl. Phys. Lett.* **2013**, *102*, 163904(1)−163904(5).
(9) Yu, K. J.; Gao, L.; Park, J. S.; Lee, Y. R.; Corcoran, C. J.; Nuzzo, R. G.; Chanda, D.; Rogers, J. A. Light Trapping in Ultrathin Monocrystalline Silicon Solar Cells. *Adv. Energy Mater.* **2013**, *3*, 1401−1406.
(10) Garnett, E.; Yang, P. Light trapping in silicon nanowire solar cells. *Nano Lett.* **2010**, *10*, 1082−1087.
(11) Wong, S.-M.; Yu, H.-Y.; Li, Y.; Li, J.; Sun, X.-W.; Singh, N.; Lo, P. G. Q.; Kwong, D.-L. Boosting Short-Circuit Current With Rationally Designed Periodic Si Nanopillar Surface Texturing for Solar Cells. *IEEE Trans. Electron Devices* **2011**, *58*, 3224−3229.
(12) Pudasaini, P. R.; Ruiz-Zepeda, F.; Sharma, M.; Elam, D.; Ponce, A.; Ayon, A. A. High efficiency hybrid silicon nanopillar-polymer solar cells. *ACS Appl. Mater. Interfaces* **2013**, *5*, 9620−9627.
(13) Shen, X.; Sun, B.; Liu, D.; Lee, S. T. Hybrid heterojunction solar cell based on organic−inorganic silicon nanowire array architecture. *J. Am. Chem. Soc.* **2011**, *133*, 19408−19415.
(14) Wang, W. C.; Lin, C. W.; Chen, H. J.; Chang, C. W.; Huang, J. J.; Yang, M. J.; Tjahjono, B.; Huang, J. J.; Hsu, W. C.; Chen, M. J. Surface passivation of efficient nanotextured black silicon solar cells using thermal atomic layer deposition. *ACS Appl. Mater. Interfaces* **2013**, *5*, 9752−9759.
(15) Pudasaini, P. R.; Elam, D.; Ayon, A. A. Aluminum oxide passivated radial junction sub-micrometre pillar array textured silicon solar cells. *J. Phys. D: Appl. Phys.* **2013**, *46*, 235104(1)−235104(8).
(16) Tsakalakos, L.; Balch, J.; Fronheiser, J.; Korevaar, B. A.; Sulima, O.; Rand, J. Silicon nanowire solar cells. *Appl. Phys. Lett.* **2007**, *91*, 233117(1)−233117(3).
(17) Shir, D.; Yoon, J.; Chanda, D.; Ryu, J. H.; Rogers, J. A. Performance of ultrathin silicon solar microcells with nanostructures of relief formed by soft imprint lithography for broad band absorption enhancement. *Nano Lett.* **2010**, *10*, 3041−3046.
(18) Jeong, S.; Garnett, E. C.; Wang, S.; Yu, Z.; Fan, S.; Brongersma, M. L.; McGehee, M. D.; Cui, Y. Hybrid silicon nanocone−polymer solar cells. *Nano Lett.* **2012**, *12*, 2971−2976.
(19) Wang, B.; Leu, P. W. Enhanced absorption in silicon nanocone arrays for photovoltaics. *Nanotechnology* **2012**, *23*, 194003(1)−194003(7).
(20) Peng, K.-Q.; Wang, X.; Li, L.; Wu, X.-L.; Lee, S.-T. High-Performance Silicon Nanohole Solar Cells. *J. Am. Chem. Soc.* **2010**, *132*, 6872−6873.
(21) Chen, T.-G.; Yu, P.; Chen, S.-W.; Chang, F.-Y.; Huang, B.-Y.; Cheng, Y.-C.; Hsiao, J.-C.; Li, C.-K.; Wu, Y.-R. Characteristics of large-scale nanohole arrays for thin-silicon photovoltaics. *Prog. Photovolt.: Res. Appl.* **2012**, DOI: 10.1002/pip.2291.
(22) Pudasaini, P. R.; Ayon, A. A. Nanostructured thin film silicon solar cells efficiency improvement using gold nanoparticles. *Phys. Status Solidi A* **2012**, *209*, 1475−1480.
(23) Han, S. E.; Chen, G. Toward the Lambertian limit of light trapping in thin nanostructured silicon solar cells. *Nano Lett.* **2010**, *10*, 4692−4696.
(24) Han, S. E.; Chen, G. Optical absorption enhancement in silicon nanohole arrays for solar photovoltaics. *Nano Lett.* **2010**, *10*, 1012−1015.
(25) Syu, H.-J.; Shiu, S.-C.; Hung, Y., Jr.; Hsueh, C.-C.; Lin, T.-C.; Subramani, T.; Lee, S.-L.; Lin, C.-F. Influences of silicon nanowire morphology on its electro-optical properties and applications for hybrid solar cells. *Prog. Photovolt.: Res. Appl.* **2013**, *21*, 1400−1410.
(26) Tseng, P.-C.; Yu, P.; Chen, H.-C.; Tsai, Y.-L.; Han, H.-W.; Tsai, M.-A.; Chang, C.-H.; Kuo, H.-C. Angle-resolved characteristics of silicon photovoltaics with passivated conical-frustum nanostructures. *Sol. Energy Mater. Sol. Cells* **2011**, *95*, 2610−2615.
(27) Li, Y.; Yu, H.; Li, J.; Wong, S. M.; Sun, X. W.; Li, X.; Cheng, C.; Fan, H. J.; Wang, J.; Singh, N.; Lo, P. G.; Kwong, D. L. Novel silicon nanohemisphere-array solar cells with enhanced performance. *Small* **2011**, *7*, 3138−3143.
(28) Kim, D. R.; Lee, C. H.; Rao, P. M.; Cho, I. S.; Zheng, X. Hybrid Si microwire and planar solar cells: passivation and characterization. *Nano Lett.* **2011**, *11*, 2704−2708.
(29) Spinelli, P.; Ferry, V. E.; van de Groep, J.; van Lare, M.; Verschuuren, M. A.; Schropp, R. E. I.; Atwater, H. A.; Polman, A. Plasmonic light trapping in thin-film Si solar cells. *J. Opt.* **2012**, *14*, 024002(1)−024002(11).
(30) Atwater, H. A.; Polman, A. Plasmonics for improved photovoltaic devices. *Nat. Mater.* **2010**, *9*, 205−213.
(31) Ouyang, Z.; Zhao, X.; Varlamov, S.; Tao, Y.; Wong, J.; Pillai, S. Nanoparticle-enhanced light trapping in thin-film silicon solar cells. *Prog. Photovolt.: Res. Appl.* **2011**, *19*, 917−926.
(32) Beck, F. J.; Mokkapati, S.; Catchpole, K. R. Plasmonic light-trapping for Si solar cells using self-assembled, Ag nanoparticles. *Prog. Photovolt.: Res. Appl.* **2010**, *18*, 500−504.
(33) Tan, H.; Santbergen, R.; Smets, A. H.; Zeman, M. Plasmonic light trapping in thin-film silicon solar cells with improved self-assembled silver nanoparticles. *Nano Lett.* **2012**, *12*, 4070−4076.
(34) Hägglund, C.; Apell, S. P. Plasmonic Near-Field Absorbers for Ultrathin Solar Cells. *J. Phys. Chem. Lett.* **2012**, *3*, 1275−1285.
(35) Yang, Y.; Pillai, S.; Mehrvarz, H.; Kampwerth, H.; Ho-Baillie, A.; Green, M. A. Enhanced light trapping for high efficiency crystalline solar cells by the application of rear surface plasmons. *Sol. Energy Mater. Sol. Cells* **2012**, *101*, 217−226.
(36) Huynh, W. U.; Dittmer, J. J.; Alivisatos, A. P. Hybrid nanorod-polymer solar cells. *Science* **2002**, *295*, 2425−2427.
(37) Avasthi, S.; Lee, S.; Loo, Y. L.; Sturm, J. C. Role of majority and minority carrier barriers silicon/organic hybrid heterojunction solar cells. *Adv. Mater.* **2011**, *23*, 5762−5766.
(38) Wei, W. R.; Tsai, M. L.; Ho, S. T.; Tai, S. H.; Ho, C. R.; Tsai, S. H.; Liu, C. W.; Chung, R. J.; He, J. H. Above-11%-efficiency organic-inorganic hybrid solar cells with omnidirectional harvesting characteristics by employing hierarchical photon-trapping structures. *Nano Lett.* **2013**, *13*, 3658−3663.
(39) Zhang, F.; Liu, D.; Zhang, Y.; Wei, H.; Song, T.; Sun, B. Methyl/allyl monolayer on silicon: efficient surface passivation for silicon-conjugated polymer hybrid solar cell. *ACS Appl. Mater. Interfaces* **2013**, *5*, 4678−4684.
(40) He, L.; Jiang, C.; Wang, H.; Lai, D.; Rusli. Si nanowires organic semiconductor hybrid heterojunction solar cells toward 10% efficiency. *ACS Appl. Mater. Interfaces* **2012**, *4*, 1704−1708.
(41) Lee, M. M.; Teuscher, J.; Miyasaka, T.; Murakami, T. N.; Snaith, H. J. Efficient hybrid solar cells based on meso-superstructured organometal halide perovskites. *Science* **2012**, *338*, 643−647.
(42) Huang, Z.; Geyer, N.; Werner, P.; de Boor, J.; Gosele, U. Metal-assisted chemical etching of silicon: a review. *Adv. Mater.* **2011**, *23*, 285−308.
(43) Qi, Y.; Wang, Z.; Zhang, M.; Yang, F.; Wang, X. A Processing Window for Fabricating Heavily Doped Silicon Nanowires by Metal-Assisted Chemical Etching. *J. Phys. Chem. C* **2013**, *117*, 25090−25096.

(44) Chartier, C.; Bastide, S.; Lévy-Clément, C. Metal-assisted chemical etching of silicon in HF–H_2O_2. *Electrochim. Acta* **2008**, *53*, 5509–5516.
(45) Mikhael, B.; Elise, B.; Xavier, M.; Sebastian, S.; Johann, M.; Laetitia, P. New silicon architectures by gold-assisted chemical etching. *ACS Appl. Mater. Interfaces* **2011**, *3*, 3866–3873.
(46) Liang, H.; Wang, W.; Huang, Y.; Zhang, S.; Wei, H.; Xu, H. Controlled Synthesis of Uniform Silver Nanospheres. *J. Phys. Chem. C* **2010**, *114*, 7427–7431.
(47) Air mass 1.5G Spectra, American Society for Testing and Materials, http://rredc.nrel.gov/solar/spectra/am1.5/ (accessed Dec 15, 2013).